Microphysical analysis for peristaltic flow of SWCNT and MWCNT carbon nanotubes inside a catheterised artery having thrombus: irreversibility effects with entropy

Anber Saleem

Department of Anatomy School of Dentistry,
Shaheed Zulifqar Ali Bhutto Medical University Islamabad, Pakistan
Email: anber.saleem@tdtu.edu.vn

Salman Akhtar and Sohail Nadeem*

Department of Mathematics,
Quaid-i-Azam University,
45320, Islamabad 44000, Pakistan
Email: salman.awan148@gmail.com
Email: sohail@qau.edu.pk
*Corresponding author

Mehdi Ghalambaz

Institute of Research and Development,
Duy Tan University,
Da Nang 550000, Vietnam
and
Faculty of Electrical – Electronic Engineering,
Duy Tan University,
Da Nang 550000, Vietnam
Email: mehdighalambaz@duytan.edu.vn

Abstract: The blood flow with carbon nanotubes, examining study case of both single and multi-wall carbon nanotubes is mathematically interpreted. The blood vessel has a sinusoidally fluctuating outer wall and a thrombus is placed at the centre. The restriction to flow is improved by application of a catheter. Entropy is also examined to interpret the irreversibility results. The final results are explained with graphs for exactly obtained mathematical solutions. Streamlines are drawn and they clearly show sinusoidally fluctuating wall on one side and a thrombus on the other side at the centre.

Keywords: peristaltic flow; catheterised artery; thrombus; carbon nanotubes; entropy.

Reference to this paper should be made as follows: Saleem, A., Akhtar, S., Nadeem, S. and Ghalambaz, M. (2021) 'Microphysical analysis for peristaltic flow of SWCNT and MWCNT carbon nanotubes inside a catheterised artery having thrombus: irreversibility effects with entropy', *Int. J. Exergy*, Vol. 34, No. 3, pp.301–314.

Copyright © 2021 Inderscience Enterprises Ltd.

Biographical notes: Anber Saleem is working as an Associate Professor. She has published over 20 research papers in the field of physiology and anatomy. She has strong research collaboration in her field.

Salman Akhtar is doing his PhD under the supervision of Prof. Dr. Sohail Nadeem. He is excellent in research and has published more than ten papers in his field.

Sohail Nadeem is an author of more than 520 ISI papers. His citations are over 15,000 and he successfully supervised 26 PhD and more than 90 MPhil students. He is a Fellow in the Pakistan Academy of Sciences. He received many awards and honours in the field of Applied Mathematics.

Mehdi Ghalambaz is currently working in Duy Tan University Vietnam. He has published number of Q1 and Q2 category papers. He has earned a number of citations.

1 Introduction

The transportation of fluid within tubes having sinusoidally moving walls is called Peristalsis. These sinusoidally fluctuating walls contract and relax in a very organised manner that results in the movement of fluid. Barton and Raynor (1968) had interpreted the fluid flow inside tubes with sinusoidally advancing walls. The average tube radius is comparatively taken very small when compared to the wavelength of fluctuating wall. The lubrication approximation was utilised by Burns and Parkes (1967) to examine the axial symmetric flow in cylinder. Fung and Yih (1968) had provided a mathematical description of the two dimensional, Newtonian flow in cylinder with sinusoidally fluctuating walls. A viscous model for this fluid flow problem with 'no slip' conditions is taken into consideration. The main flow is developed along cylinder's axis due to this fluctuating behaviour of wavy walls along channel's length (Jaffrin and Shapiro, 1971). Takabatake et al. (1988) had considered peristaltic flow with trapping phenomena and reflux in their work. They had also evaluated the concept of efficiency and peristaltic mixing in their mathematical study. Akbarzadeh (2018) had mathematically studied the flow of biofluid inside a vessel having sinusoidally fluctuating walls.

The blood transportation to major organs of our body is restricted due to development of a thrombus inside the artery. It develops due to collection of fats, cholesterol and some other material. The flow through such diseased arteries is improved by utilising a catheter. That is a hollow, narrow, fine tube inserted in such diseased arteries and finally it improves the flow. The peristalsis mechanism can also happen within vessel having short lengths, as the diameter of such vessels alters systematically due to vasomotion. The medical and engineering applications of catheter involve urological, neurovascular, gastrointestinal procedures. Further, it is applicable in insulin pumps, measurement of blood pressure in a vein, etc. The development of a thrombus in diseased vessels is discussed in details (van Kempen et al., 2016). Doffin and Chagneau (1981) had described both, a theoretical model as well as an experimental work by using viscous Newtonian model for a diseases vessel with thrombus. The blood flow treated as micropolar fluid inside a channel with fluctuating peristaltic wall and a clot model was explained by Mekheimer and Elmaboud (2008). Srivastava and Rastogi (2010) had

studied the flow in an artery by means of a catheter, considering a two phase model for their flow problem. The couple stress model of fluid flow was utilised by Reddy et al. (2014) to interpret the blood flow by application of a catheter in a diseased narrow artery. Further, reference for blood flow problem is provided (Uddin et al., 2020).

In many industrial and engineering applications that are connected to fluid mechanics, the transfer of heat phenomenon is limited due to some fluid with small thermal conductivity. Thus the required thermal conductivity for such flow problems is achieved by using nanoparticles in the flow (Choi and Eastman, 1995). The nanofluid flow between two concentric tubes was mathematically investigated by Akbar and Nadeem (2011). The flow of carbon nanotubes inside a channel having sinusoidally fluctuating wall was also interpreted by Akbar et al. (2015). Shahzadi and Nadeem (2017) had investigated the nanofluid flow in an inclined tube having wavy walls with a thrombus at centre.

The transfer of heat is fully explained by considering viscous effects together with entropy. The disturbance and chaos in a system is entropy. The transfer of heat for flow in circular channel having sinusoidally fluctuating wall, considering Phan-Thien Tanner model of fluid flow was interpreted by Butt et al. (2020). The hydrodynamic study for a permeable geometry is provided (Kahshan et al., 2019). The entropy interpretation for fluid dynamics flow problems was firstly provided by Bejan (1979). Akbar (2015) provided a theoretical study for entropy generation due to carbon nanotube flow in cylinder. Further literature review is provided for nanoparticles study problems (Kasaragadda et al., 2020; Hajizadeh et al., 2019; Souayeh et al., 2019; Chinni et al., 2019; Akermi et al., 2019). We have studied the accessible literature and it is easily revealed that the peristaltic blood flow of carbon nanotubes in a cylindrical channel having a thrombus is not explored by anyone yet mathematically. Thus, our work aims to describe the blood flow with carbon nanotubes, examining study case of both single and multi-wall carbon nanotubes in an artery with sinusoidally fluctuating outer wall and a thrombus at the centre. The restriction to flow is improved by application of a catheter. The effect of viscous dissipation is also incorporated in energy equation and entropy is also examined to interpret the irreversibility results. The final results are explained with graphs for exactly obtained mathematical solutions. Streamlines are drawn and they clearly show sinusoidally fluctuating wall on one side and a thrombus on the other side at the centre.

2 Mathematical formulation

The blood flow with carbon nanotubes, correlating the study of both single and multi-wall carbon nanotubes, is mathematically interpreted in a catheterised artery with sinusoidally fluctuating outer wall and a thrombus at the centre. Here $\vec{V} = (\bar{U}, 0, \bar{W})$ is the chosen velocity field, where the radial and axial velocities are $\bar{U}$ and $\bar{W}$.

The expressions for outer boundary $\bar{\eta}(z)$ as well as inner boundary $\bar{\epsilon}(z)$ in their dimensional form are provided by (Akbar, 2015).

$$\bar{\epsilon}(z) = \begin{cases} R_0\left[a + f_1(\bar{z})\right] & 0 \le \bar{z} \le \lambda \\ R_0^a & \text{otherwise} \end{cases} \tag{1}$$

$$\overline{\eta}(z) = R_0 + b\mathrm{Sin}\left(\frac{2\pi}{\lambda}(\overline{Z} - c\overline{t})\right), \tag{2}$$

Here $f_1(\overline{z})$ mainly handles the clot shape and it is chosen accordingly. The dimensional form of governing flow equations is given (Shahzadi and Nadeem, 2017).

$$\frac{1}{\overline{R}}\frac{\partial(\overline{R}\overline{U})}{\partial\overline{R}} + \frac{\partial(\overline{W})}{\partial\overline{Z}} = 0, \tag{3}$$

$$\rho_{nf}\left[\frac{\partial\overline{U}}{\partial\overline{t}} + \overline{U}\frac{\partial\overline{U}}{\partial\overline{R}} + \overline{W}\frac{\partial\overline{U}}{\partial\overline{Z}}\right] = -\frac{\partial\overline{P}}{\partial\overline{R}} + \mu_{nf}\left[\frac{\partial^2\overline{U}}{\partial\overline{R}^2} + \frac{1}{\overline{R}}\frac{\partial\overline{U}}{\partial\overline{R}} + \frac{\partial^2\overline{U}}{\partial\overline{Z}^2} - \frac{\overline{U}}{\overline{R}^2}\right], \tag{4}$$

$$\rho_{nf}\left[\frac{\partial\overline{W}}{\partial\overline{t}} + \overline{U}\frac{\partial\overline{W}}{\partial\overline{R}} + \overline{W}\frac{\partial\overline{W}}{\partial\overline{Z}}\right] = -\frac{\partial\overline{P}}{\partial\overline{Z}} + \mu_{nf}\left[\frac{\partial^2\overline{W}}{\partial\overline{R}^2} + \frac{1}{\overline{R}}\frac{\partial\overline{W}}{\partial\overline{R}} + \frac{\partial^2\overline{W}}{\partial\overline{Z}^2}\right], \tag{5}$$

$$\begin{aligned}\left(\rho C_p\right)_{nf}\left[\frac{\partial\overline{T}}{\partial\overline{t}} + \overline{U}\frac{\partial\overline{T}}{\partial\overline{R}} + \overline{W}\frac{\partial\overline{T}}{\partial\overline{Z}}\right] &= k_{nf}\left[\frac{\partial^2 T}{\partial\overline{R}^2} + \frac{1}{\overline{R}}\frac{\partial\overline{T}}{\partial\overline{R}} + \frac{\partial^2\overline{T}}{\partial\overline{Z}^2}\right] \\ +\mu_{nf}\left[2\left\{\left(\frac{\partial\overline{U}}{\partial\overline{R}}\right)^2 + \left(\frac{\overline{U}}{\overline{R}}\right)^2 + \left(\frac{\partial\overline{W}}{\partial\overline{Z}}\right)^2\right\} + \left(\frac{\partial\overline{U}}{\partial\overline{Z}} + \frac{\partial\overline{W}}{\partial\overline{R}}\right)^2\right],\end{aligned} \tag{6}$$

The dimensional form of boundary conditions is provided in fixed frame

$$\begin{aligned}&\overline{W} = 0 \text{ at } \overline{R} = \overline{\epsilon}(z) \text{ and } \overline{W} = 0, \text{ at } \overline{R} = \overline{\eta}(z). \\ &\overline{T} = \overline{T}_1 \text{ at } \overline{R} = \overline{\epsilon}(z) \text{ and } \overline{T} = \overline{T}_0 \text{ at } \overline{R} = \overline{\eta}(z).\end{aligned} \tag{7}$$

The frame is shifted from fixed $(\overline{R}, \overline{Z})$ to moving $(\overline{r}, \overline{z})$ frame by application of these transformations.

$$\overline{z} = \overline{Z} - c\overline{t},\ \overline{w} = \overline{W} - c,\ \overline{p}(\overline{z}, \overline{r}) = \overline{P}(\overline{Z}, \overline{R}, \overline{t}),\ \overline{r} = \overline{R},\ \overline{u} = \overline{U}, \tag{8}$$

The dimensionless variables are

$$\begin{aligned}&r = \frac{\overline{r}}{R_0},\ z = \frac{\overline{z}}{\lambda},\ u = \frac{\lambda\overline{u}}{R_0 c},\ w = \frac{\overline{w}}{c},\ t = \frac{c\overline{t}}{\lambda},\ p = \frac{R_0^2\overline{p}}{c\lambda\mu_f},\ \theta = \frac{\overline{T} - \overline{T}_0}{\overline{T}_1 - \overline{T}_0}, \\ &\epsilon(z) = \frac{\overline{\epsilon}(z)}{R_0},\ \eta(z) = \frac{\overline{\eta}(z)}{R_0},\ \psi = \frac{b}{R_0},\ B_r = \frac{c^2\mu_f}{\left(T_1 - \overline{T}_0\right)k_f},\ \theta_0 = \frac{\overline{T}_0}{\overline{T}_1 - \overline{T}_0}, \\ &S_{G_0} = \frac{k_f\left(\overline{T}_1 - \overline{T}_0\right)^2}{\overline{T}_0^2 R_0^2},\end{aligned} \tag{9}$$

The equations (3) to (7) are simplified by using equations (8) and (9), to get these dimensionless equations

$$\frac{1}{r}\frac{\partial(ru)}{\partial r} + \frac{\partial w}{\partial z} = 0, \tag{10}$$

$$\frac{\partial p}{\partial r} = 0, \tag{11}$$

$$\frac{\partial p}{\partial z}=\frac{\mu_{nf}}{\mu_f}\left(\frac{\partial^2 w}{\partial r^2}+\frac{1}{r}\frac{\partial w}{\partial r}\right), \tag{12}$$

$$\frac{k_{nf}}{k_f}\left(\frac{\partial^2 \theta}{\partial r^2}+\frac{1}{r}\frac{\partial \theta}{\partial r}\right)+\frac{\mu_{nf}}{\mu_f}B_r\left(\frac{\partial w}{\partial r}\right)^2=0, \tag{13}$$

With corresponding dimensionless boundary conditions

$$w=-1 \text{ at } r=\epsilon(z) \text{ and } w=-1 \text{ at } r=\eta(z). \tag{14}$$

$$\theta=1 \text{ at } r=\epsilon(z) \text{ and } \theta=0 \text{ at } r=\eta(z). \tag{15}$$

The dimensionless expression for outer $\eta(z)$ as well as inner boundary $\epsilon(z)$ is given and $f_1(\bar{z})$ is accordingly selected as (Jayaraman and Sarkar, 2005).

$$\epsilon(z)=\begin{cases} a+\sigma e^{-\pi^2(z-z_d-0.5)^2}, & 0\le z\le 1 \\ a, & \text{otherwise} \end{cases}, \tag{16}$$

$$\eta(z)=1+\psi \text{Sin}(2\pi z), \tag{17}$$

3 Exact solution

Equation (12) is solved with conditions given in equation (14), to get exact solution for velocity

$$w=\frac{\left[\frac{\partial p}{\partial z}\left(\epsilon^2+\eta^2\right)\text{Log}(r)+\left(\frac{\partial p}{\partial z}\left(r^2-\eta^2\right)-4\frac{\mu_{nf}}{\mu_f}\right)\text{Log}(\epsilon)+\left(\frac{\partial p}{\partial z}(\epsilon^2-r^2)+4\frac{\mu_{nf}}{\mu_f}\right)\text{Log}(\eta)\right]}{4\frac{\mu_{nf}}{\mu_f}\left(\text{Log}(\epsilon)-\text{Log}(\eta)\right)}, \tag{18}$$

The volumetric rate of flow is evaluated by using

$$Q=\int_{\epsilon}^{\eta} rw dr, \tag{19}$$

The result for pressure gradient expression is calculated as

$$\frac{dp}{dz}=\frac{8\left(2Q-\epsilon^2+\eta^2\right)\frac{\mu_{nf}}{\mu_f}\left(\text{Log}(\epsilon)-\text{Log}(\eta)\right)}{\left(\epsilon^2-\eta^2\right)\left[-\epsilon^2+\eta^2+\left(\epsilon^2+\eta^2\right)\left(\text{Log}(\epsilon)-\text{Log}(\eta)\right)\right]}, \tag{20}$$

The wall shear stress τ_w is obtained as

$$\tau_w = \frac{\partial w}{\partial r}\bigg|_{r=\eta} = -\frac{\dfrac{dp}{dz}\left(\epsilon^2+\eta^2\right)}{\eta} + 2\frac{dp}{dz}\eta\left(\mathrm{Log}(\epsilon)-\mathrm{Log}(\eta)\right)}{4\dfrac{\mu_{nf}}{\mu_f}\left(\mathrm{Log}(\epsilon)-\mathrm{Log}(\eta)\right)}, \tag{21}$$

Figure 1 Geometry of the problem (see online version for colours)

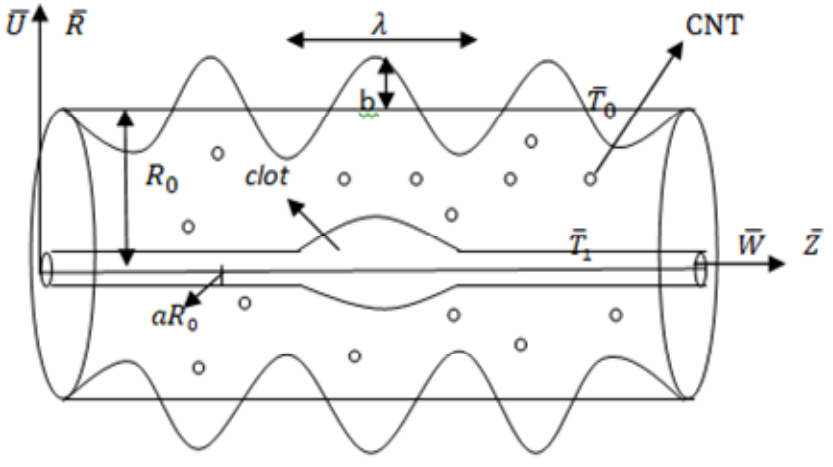

Equation (13) is solved with conditions given in equation (15), to get exact temperature solution

$$\begin{aligned}
\theta = \frac{1}{64\dfrac{k_{nf}}{k_f}\dfrac{\mu_{nf}}{\mu_f}\left(\mathrm{Log}(\epsilon)-\mathrm{Log}(\eta)\right)^2}\Bigg[& -2B_r\left(\frac{dp}{dz}\right)^2\left(\epsilon^2-\eta^2\right)\left(\mathrm{Log}(r)\right)^2 \\
& -B_r\left(\frac{dp}{dz}\right)^2\left(r^2-\eta^2\right)\mathrm{Log}(\epsilon)\left\{-4\left(\epsilon^2-\eta^2\right)+\left(r^2+\eta^2\right)\mathrm{Log}(\epsilon)\right\} \\
& +\Bigg\{-4B_r\left(\frac{dp}{dz}\right)^2\left(r^2-\epsilon^2\right)\left(\epsilon^2-\eta^2\right)+\left(B_r\left(\frac{dp}{dz}\right)^2\left(2r^4-3\epsilon^4\right.\right. \\
& \left.\left.+4\epsilon^2\eta^2-3\eta^4\right)-64\frac{k_{nf}}{k_f}\frac{\mu_{nf}}{\mu_f}\right)Log(\epsilon)\Bigg\}\mathrm{Log}(\eta)+\left(B_r\left(\frac{dp}{dz}\right)^2\left(-r^4+\epsilon^4\right)\right. \\
& \left.+64\frac{k_{nf}}{k_f}\frac{\mu_{nf}}{\mu_f}\right)\left(\mathrm{Log}(\eta)\right)^2+\mathrm{Log}(r)\Bigg\{-4B_r\left(\frac{dp}{dz}\right)^2\left(\epsilon^2-\eta^2\right)^2 \\
& +\left(B_r\left(\frac{dp}{dz}\right)^2\left(3\epsilon^4-4\epsilon^2\eta^2+\eta^4\right)+64\frac{k_{nf}}{k_f}\frac{\mu_{nf}}{\mu_f}\right)\mathrm{Log}(\epsilon) \\
& +\left(B_r\left(\frac{dp}{dz}\right)^2\left(\epsilon^4-4\epsilon^2\eta^2+3\eta^4\right)-64\frac{k_{nf}}{k_f}\frac{\mu_{nf}}{\mu_f}\right)\mathrm{Log}(\eta)\Bigg\}\Bigg],
\end{aligned} \tag{22}$$

Table 1 CNT model

Density	$\rho_{nf} = (1-\phi)\,\rho_f + \phi\rho_{CNT}$
Heat capacity	$(\rho C_p)_{nf} = (1-\phi)\,(\rho C_p)_f + \phi(\rho C_p)_{CNT}$
Viscosity	$\frac{\mu_{nf}}{\mu_f} = \frac{1}{(1-\phi)^{2.5}}$
Thermal conductivity	$\frac{k_{nf}}{k_f} = \frac{1-\phi+2\phi\left(\frac{k_{CNT}}{k_{CNT}-k_f}\right)\mathrm{Log}\left(\frac{k_{CNT}+k_f}{2k_f}\right)}{1-\phi+2\phi\left(\frac{k_f}{k_{CNT}-k_f}\right)\mathrm{Log}\left(\frac{k_{CNT}+k_f}{2k_f}\right)}$

Source: Akbar (2014)

Table 2 Thermo physical properties of base fluid and CNT's

Physical parameter	*Base fluid (f) blood*	*SWCNT*	*MWCNT*
ρ	1,063	2,600	1,600
k	0.492	6,600	3,000
C_p	3,617	425	796

Source: Akbar (2014)

4 Entropy generation analysis

The dimensional form of expression for entropy equation is provided as (Bejan, 1979)

$$S_G = \frac{k_{nf}}{\bar{T}_0^2}\left[\left(\frac{\partial \bar{T}}{\partial \bar{r}}\right)^2 + \left(\frac{\partial \bar{T}}{\partial \bar{z}}\right)^2\right] + \frac{\mu_{nf}}{\bar{T}_0}\left[2\left\{\left(\frac{\partial \bar{u}}{\partial \bar{r}}\right) + \left(\frac{\bar{u}}{\bar{r}}\right)^2 + \left(\frac{\partial \bar{w}}{\partial \bar{z}}\right)^2\right\} + \left(\frac{\partial \bar{w}}{\partial \bar{r}} + \frac{\partial \bar{u}}{\partial \bar{z}}\right)\right], \quad (23)$$

The dimensionless expression for entropy generation is obtained by application of dimensionless variables that are provided in equation (9).

$$N_S = \frac{S_G}{S_{G_0}} = \frac{k_{nf}}{k_f}\left(\frac{\partial \theta}{\partial r}\right)^2 + \frac{\mu_{nf}}{\mu_f}\theta_0 B_r\left(\frac{\partial w}{\partial r}\right)^2, \quad (24)$$

There are two portions of equation (24), the initial one is entropy developed because of limited temperature difference $(N_{S_{cond}})$ whereas the later one explains the entropy developed because of viscous effects $(N_{S_{visc}})$. Bejan (1979) number is incorporated by

$$B_e = \frac{N_{S_{cond}}}{N_{S_{cond}} + N_{S_{visc}}}, \quad (25)$$

5 Results and discussion

This segment incorporates the graphical illustration of results that are found in previous section. Combined graphical results are developed for both cases of carbon nanotubes.

The effects of various parameters on velocity of flow, temperature and irreversibility are discussed. The graphs for velocity are plotted against parameters Q and σ as shown in Figures 2(a)–2(b). Figure (2a) reveals that as the value of Q increment, the velocity gains magnitude for both carbon nanotubes. The velocity of flow decreases with clot wall as the height σ of clot enhances but it shows constant behaviour with fluctuating peristaltic wall as depicted in Figure 2(b). The velocity declines at clot surface with increasing clot height due to 'no slip' condition at boundaries but velocity remains same at peristaltic surface. It is clearly seen in these graphs of velocity that the plotted curves for both cases of carbon nanotubes overlap. The reason is independence of velocity profile from CNT's thermo physical properties and it only involves the concentration term. In Figures 3(a)–3(d) the temperature for this flow problem is plotted for distinct parameters of interest. There is increment in temperature as value of B_r enhances, as displayed in Figure 3(a). It conveys that conduction heat transfer is less when compared to heat produced by viscous effects. Further, the temperature enhances quickly in case of MWCNT when compared with SWCNT. The temperature of base fluid decreases with incrementing the concentration ϕ of nanofluid as shown in Figure 3(b). It is clear from here that carbon nanotubes concentration is basically used to control the heat transfer mechanism. As the value of Q enhances, the temperature increments as depicted in Figure 3(c). It is notable that by incrementing Q, there is enhance in both velocity as well as temperature. As the height σ of clot increments, there is increase in the temperature, as given in Figure 3(d). Moreover, the temperature enhances rapidly for MWCNT when compared with SWCNT. The shear stress τ_w at outer wall is plotted against z-axis, as given in Figures 4(a)–4(b). In both cases of study (i.e., SWCNT as well as MWCNT) τ_w increments with enhancing Q, as shown in Figure 4(a). Mainly, it gains magnitude due to 'no slip' at boundaries. Also, τ_w enhances with incrementing height σ of clot, as revealed in Figure 4(b). The irreversibility is interpreted by plotting graphs for entropy and revealed in Figures 5(a)–5(d). Entropy has opposite behaviour with opposite walls, as depicted in Figure 5(a). Since there is increment in the entropy at sinusoidally fluctuating wall and it reduces at wall with thrombus for increasing B_r. Also there is a rapid and more enhance in entropy at sinusoidally fluctuationg wall but comparatively slow and less enhance with thrombus wall. Figure 5(b) convey that N_s enhances with thrombus wall and it reduces with wall having travelling wave with incrementing ϕ. Figure 5(c) reveals that N_s reduces with thrombus wall but gains magnitude with peristaltic wall with enhancing Q. Further, entropy increases for enhancing θ_0, as conveyed in Figure 5(d). These graphs reveal that there is least entropy at centre due to less disorder here. In Figures 6(a)–6(d), Bejan number is plotted against distinct parameters. Figure 6(a) convey that B_e decreases with thrombus wall but it attains high value at sinusoidal wall for increasing value of B_r. The value of B_e gains magnitude with wall having thrombus but there is decrease in it at peristaltic wall for enhancing ϕ, as shown in Figure 6(b). Figure 6(c) conveys that B_e reduces with wall having clot but it increments with peristaltic wall for increasing Q. Figure 6(d) depicts that B_e declines with incrementing value of θ_0. Figures 7(a)–7(d) show the streamlines plotted for this flow problem. It is clearly depicted in these streamline graphs that upper end has a sinusoidally fluctuating wall and lower end has a thrombus at the centre. Further, it is noted that closed shape streamlines increase in size with incrementing value of Q.

Figure 2 (a) Velocity for Q (b) Velocity for σ (see online version for colours)

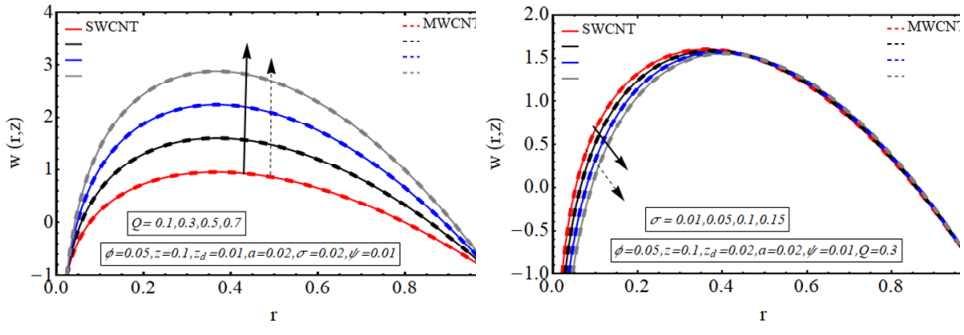

(a) (b)

Figure 3 (a) Temperature for B_r (b) Temperature for ϕ (c) Temperature for Q (d) Temperature for σ (see online version for colours)

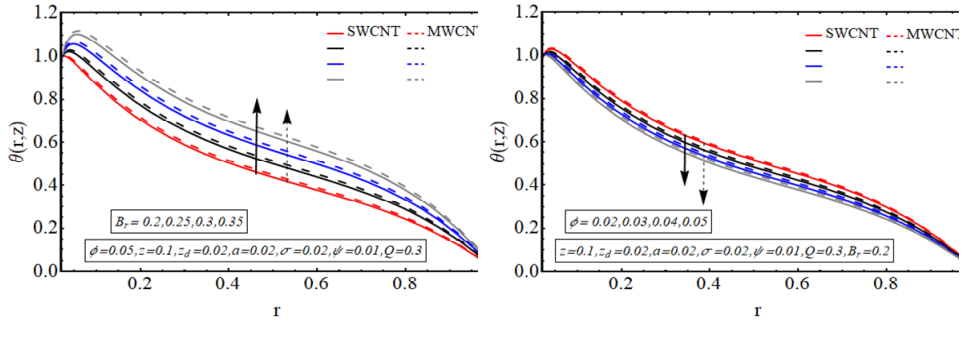

(a) (b)

Figure 3 (a) Temperature for B_r (b) Temperature for ϕ (c) Temperature for Q (d) Temperature for σ (continued) (see online version for colours)

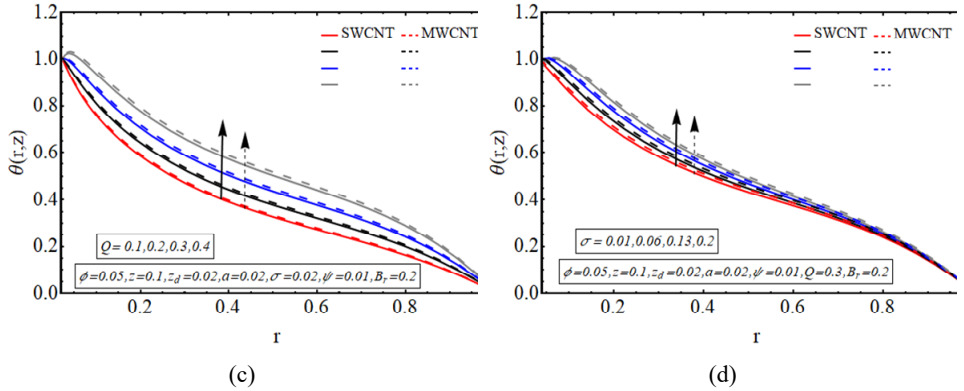

(c) (d)

Figure 4 (a) Wall shear stress for Q (b) Wall shear stress for σ (see online version for colours)

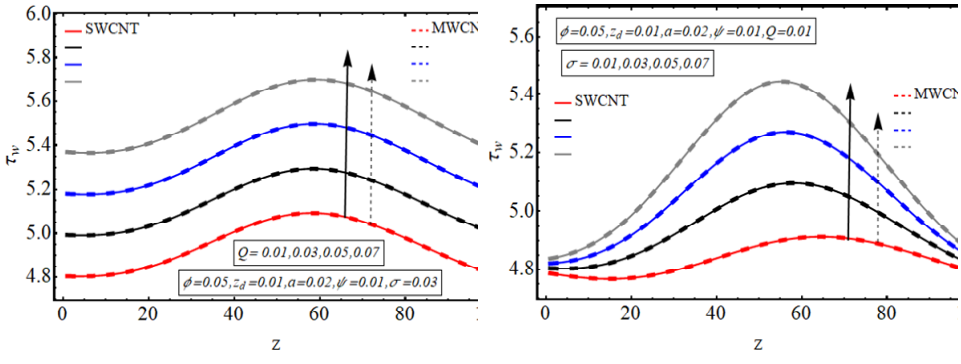

(a) (b)

Figure 5 (a) Entropy generation for B_r (b) Entropy generation for ϕ (c) Entropy generation for Q (d) Entropy generation for θ_0 (see online version for colours)

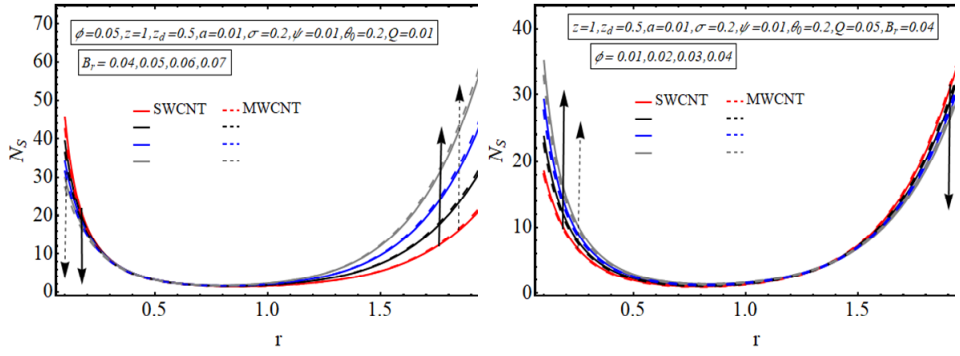

(a) (b)

Figure 5 (a) Entropy generation for B_r (b) Entropy generation for ϕ (c) Entropy generation for Q (d) Entropy generation for θ_0 (continued) (see online version for colours)

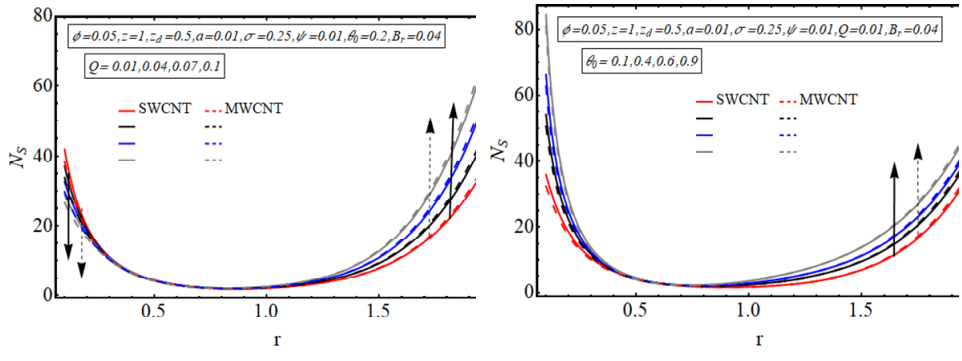

(c) (d)

Figure 6 (a) Bejan number for B_r (b) Bejan number for ϕ (c) Bejan number for Q (d) Bejan number for θ_0 (see online version for colours)

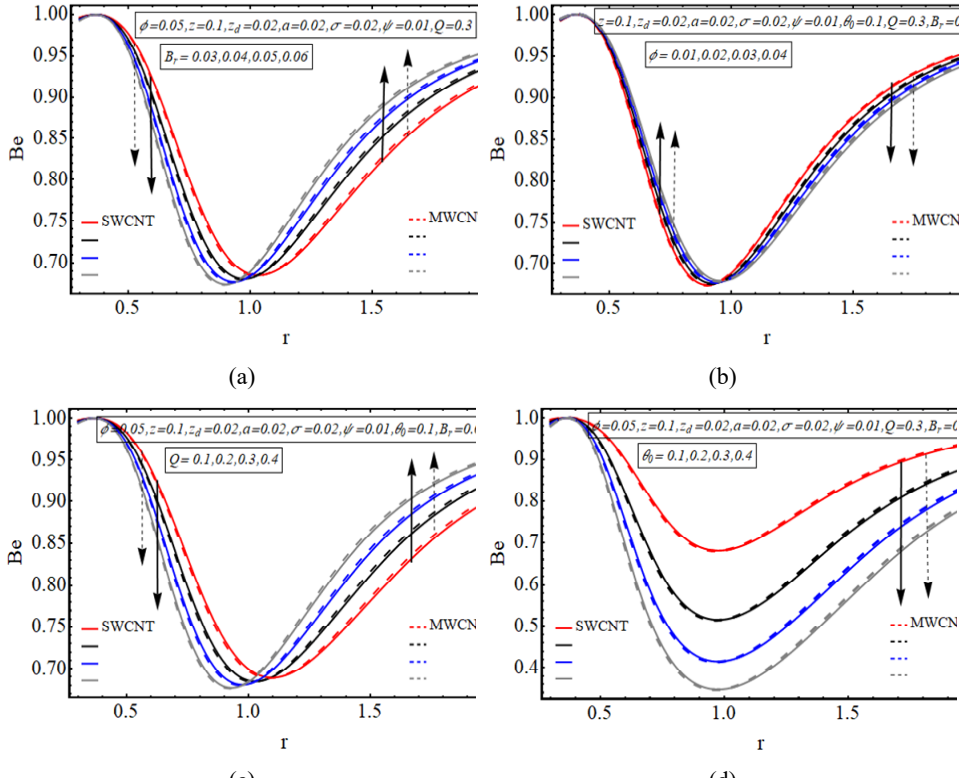

Figure 7 (a) Streamlines at $Q = 0.2$ (b) Streamlines at $Q = 0.3$ (c) Streamlines at $Q = 0.35$ (d) Streamlines at $Q = 0.4$ (see online version for colours)

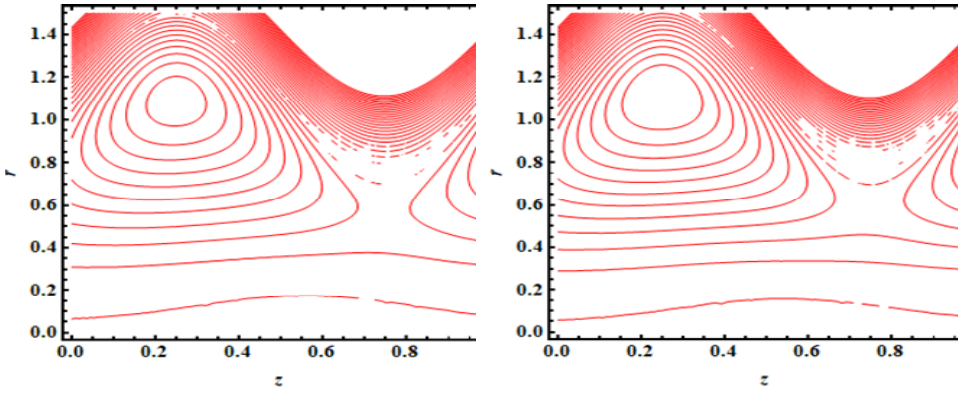

Figure 7 (a) Streamlines at $Q = 0.2$ (b) Streamlines at $Q = 0.3$ (c) Streamlines at $Q = 0.35$ (d) Streamlines at $Q = 0.4$ (continued) (see online version for colours)

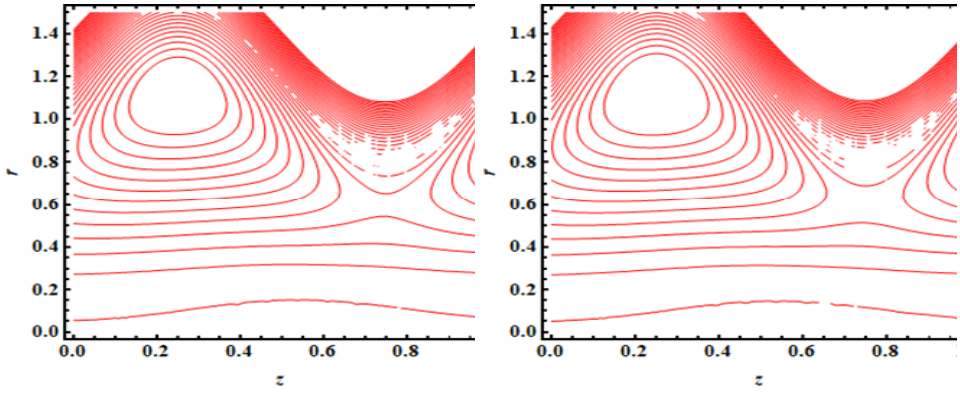

(c) (d)

6 Conclusions

The blood flow with carbon nanotubes, examining study case of both single and multi-wall carbon nanotubes, is mathematically interpreted. The blood vessel has a sinusoidally fluctuating outer wall and a thrombus is placed at the centre. The restriction to flow is improved by application of a catheter. The final conclusions are provided as

- The velocity of flow decreases with clot wall as the height σ of clot enhances but it shows constant behaviour with fluctuating peristaltic wall.
- The temperature enhances quickly in case of MWCNT when related to SWCNT.
- The base fluid temperature decreases with incrementing the concentration ϕ of nanofluid. It is clear from here that carbon nanotubes concentration is mainly used to control heat transfer.
- Entropy shows fully opposite pattern for opposite walls.
- Streamline graphs show that upper end has a sinusoidally fluctuating wall and lower end has a thrombus at the centre. Further, it is noted that closed shape streamlines enlarge with incrementing value of Q.

References

Akbar, N.S. (2014) 'MHD peristaltic flow with carbon nanotubes in an asymmetric channel', *Journal of Computational and Theoretical Nanoscience*, Vol. 11, No. 5, pp.1323–1329.

Akbar, N.S. (2015) 'Entropy generation analysis for a CNT suspension nanofluid in plumb ducts with peristalsis', *Entropy*, Vol. 17, No. 3, pp.1411–1424.

Akbar, N.S. and Nadeem, S. (2011) 'Endoscopic effects on peristaltic flow of a nanofluid', *Communications in Theoretical Physics*, Vol. 56, No. 4, p.761.

Akbar, N.S., Raza, M. and Ellahi, R. (2015) 'Influence of induced magnetic field and heat flux with the suspension of carbon nanotubes for the peristaltic flow in a permeable channel', *Journal of Magnetism and Magnetic Materials*, Vol. 381, pp.405–415.

Akbarzadeh, P. (2018) 'Peristaltic biofluids flow through vertical porous human vessels using third-grade non-Newtonian fluids model', *Biomechanics and Modeling in Mechanobiology*, Vol. 17, No. 1, pp.71–86.

Akermi, M., Jaballah, N., Alarifi, I.M., Rahimi-Gorji, M., Chaabane, R.B., Ouada, H.B. and Majdoub, M. (2019) 'Synthesis and characterization of a novel hydride polymer P-DSBT/ZnO nano-composite for optoelectronic applications', *Journal of Molecular Liquids*, Vol. 287, p.110963.

Barton, C. and Raynor, S. (1968) 'Peristaltic flow in tubes', *The Bulletin of Mathematical Biophysics*, Vol. 30, No. 4, pp.663–680.

Bejan, A. (1979) *A Study of Entropy Generation in Fundamental Convective Heat Transfer*.

Burns, J.C. and Parkes, T. (1967) 'Peristaltic motion', *Journal of Fluid Mechanics*, Vol. 29, No. 4, pp.731–743.

Butt, A.W., Akbar, N.S. and Mir, N.A. (2020) 'Heat transfer analysis of peristaltic flow of a Phan-Thien-Tanner fluid model due to metachronal wave of cilia', *Biomechanics and Modeling in Mechanobiology*, pp.1–9.

Chinni, G., Alarifi, I.M., Rahimi-Gorji, M. and Asmatulu, R. (2019) 'Investigating the effects of process parameters on microalgae growth, lipid extraction, and stable nanoemulsion productions', *Journal of Molecular Liquids*, Vol. 291, p.111308.

Choi, S.U. and Eastman, J.A. (1995) *Enhancing Thermal Conductivity of Fluids with Nanoparticles*, No. ANL/MSD/CP-84938, CONF-951135-29, Argonne National Lab., IL, USA.

Doffin, J. and Chagneau, F. (1981) 'Oscillating flow between a clot model and a stenosis', *Journal of Biomechanics*, Vol. 14, No. 3, pp.143–148.

Fung, Y.C. and Yih, C.S. (1968) *Peristaltic Transport*.

Hajizadeh, A., Shah, N.A., Shah, S.I.A., Animasaun, I.L., Rahimi-Gorji, M. and Alarifi, I.M. (2019) 'Free convection flow of nanofluids between two vertical plates with damped thermal flux', *Journal of Molecular Liquids*, Vol. 289, p.110964.

Jaffrin, M.Y. and Shapiro, A.H. (1971) 'Peristaltic pumping', *Annual Review of Fluid Mechanics*, Vol. 3, No. 1, pp.13–37.

Jayaraman, G. and Sarkar, A. (2005) 'Nonlinear analysis of arterial blood flow – steady streaming effect', *Nonlinear Analysis: Theory, Methods & Applications*, Vol. 63, Nos. 5–7, pp.880–890.

Kahshan, M., Lu, D. and Rahimi-Gorji, M. (2019) 'Hydrodynamical study of flow in a permeable channel: application to flat plate dialyzer', *International Journal of Hydrogen Energy*, Vol. 44, No. 31, pp.17041–17047.

Kasaragadda, S., Alarifi, I.M., Rahimi-Gorji, M. and Asmatulu, R. (2020) 'Investigating the effects of surface superhydrophobicity on moisture ingression of nanofiber-reinforced bio-composite structures', *Microsystem Technologies*, Vol. 26, No. 2, pp.447–459.

Mekheimer, K.S. and Elmaboud, Y.A. (2008) 'The influence of a micropolar fluid on peristaltic transport in an annulus: application of the clot model', *Applied Bionics and Biomechanics*, Vol. 5, No. 1, pp.13–23.

Reddy, J.R., Srikanth, D. and Murthy, S.K. (2014) 'Mathematical modelling of pulsatile flow of blood through catheterized unsymmetric stenosed artery – effects of tapering angle and slip velocity', *European Journal of Mechanics-B/Fluids*, Vol. 48, pp.236–244.

Shahzadi, I. and Nadeem, S. (2017) 'Role of inclined magnetic field and copper nanoparticles on peristaltic flow of nanofluid through inclined annulus: application of the clot model', *Communications in Theoretical Physics*, Vol. 67, No. 6, p.704.

Souayeh, B., Kumar, K.G., Reddy, M.G., Rani, S., Hdhiri, N., Alfannakh, H. and Rahimi-Gorji, M. (2019) 'Slip flow and radiative heat transfer behavior of titanium alloy and ferromagnetic nanoparticles along with suspension of dusty fluid', *Journal of Molecular Liquids*, Vol. 290, p.111223.

Srivastava, V.P. and Rastogi, R. (2010) 'Blood flow through a stenosed catheterized artery: effects of hematocrit and stenosis shape', *Computers & Mathematics with Applications*, Vol. 59, No. 4, pp.1377–1385.

Takabatake, S., Ayukawa, K. and Mori, A. (1988) 'Peristaltic pumping in circular cylindrical tubes: a numerical study of fluid transport and its efficiency', *Journal of Fluid Mechanics*, Vol. 193, pp.267–283.

Uddin, S., Mohamad, M., Rahimi-Gorji, M., Roslan, R. and Alarifi, I.M. (2020) 'Fractional electro-magneto transport of blood modeled with magnetic particles in cylindrical tube without singular kernel', *Microsystem Technologies*, Vol. 26, No. 2, pp.405–414.

van Kempen, T.H., Donders, W.P., van de Vosse, F.N. and Peters, G.W. (2016) 'A constitutive model for developing blood clots with various compositions and their nonlinear viscoelastic behavior', *Biomechanics and Modeling in Mechanobiology*, Vol. 15, No. 2, pp.279–291.

Nomenclature

$(\bar{R}, \bar{Z})$	Cylindrical coordinate
$(\bar{U}, \bar{W})$	Components of radial and axial velocity
R_0 (m)	Outer tube radius
aR_0 (m)	Inner tube radius
b (m)	Wave amplitude
λ (m)	Wavelength
nf	Nano-fluid
B_r	Brickmann number
$\rho_{nf}\left(\frac{\text{kg}}{\text{m}^3}\right)$	Density of nanofluid
$k_f\left(\frac{\text{W}}{\text{mK}}\right)$	Thermal conductivity of fluid
c (m⁄s)	Speed of wave
σ	Utmost height attain by clot
z_d	Clot's axial displacement
ψ	Ratio of amplitude to mean radius
CNT	Carbon nano-tubes
SWCNT	Single-wall CNT
MWCNT	Multi-wall CNT
θ_0	Absolute to characteristic temperature difference ratio
$\mu_{nf}\left(\frac{\text{kg}}{\text{ms}}\right)$	Dynamic viscosity of nanofluid
B_e	Bejan number